ISSN (e): 2250 – 3005 || Volume, 12 || Issue, 3|| May. - June. – 2022 ||
International Journal of Computational Engineering Research (IJCER)

A Simulation Study on the Focusing of Water Surface Waves Induced by Gradient-Index Lens

Yen Jie, Ch'ng[1] and Fei Fang, Chung[2]
[1]*Undergraduate,*
School of Energy and Chemical Engineering,
[2]*Assistant Professor,*
Department of Physics,
Xiamen University Malaysia, Jalan Sunsuria, Bandar Sunsuria, 43900, Sepang, Selangor, Malaysia.
Corresponding Author: Fei Fang, Chung.

ABSTRACT
The manipulation of water waves is an interesting and important issue in coastal engineering. Diverging waves can reduce the load on coastal structures and converging waves can enhance the efficiency of wave energy harvesting. In this paper, we numerically studied the focusing of surface waves induced by a gradient-index (GRIN) lens. The effects of various wave conditions and lens structure parameters on focusing wave energy were evaluated. The errors of the focal positions obtained by the smoothed-particle hydrodynamics (SPH) simulation were all less than 5% compared with the theoretical predictions given by gradient-index optics. In addition, we found that focusing of the waves did not always imply wave amplification. Only when both the linear wave and shallow-water conditions were fulfilled were the waves amplified.

KEYWORDS:*gradient-index (GRIN) lenses, smoothed particle hydrodynamics (SPH), water surface waves, wave energy concentration*

Date of Submission: 13-06-2022 Date of acceptance: 27-06-2022

I. Introduction

Ocean waves deliver a huge amount of energy to the coast every day. This energy can be hazardous to coastal structures[1]. However, if the waves could be well-controlled, such as electromagnetic waves traveling in a waveguide, this energy could be redirected and converted into useful energy.

The pioneering work of putting the idea of manipulating water waves to the test is attributed to Mehlum and Stamnes [2]. These researchers used a submerged Fresnel-type lens to transform a diverging wave into a converging wave. Although they claimed that the observation favoured the prediction of their nonlinear theory, the efficiency of the energy focusing was not significant due to the nonlinearity. Kudo et al. [3], then tested a submerged convex and crescent-shaped plate. Their experimental results were unsatisfactory due to interference by the reflected waves. Kudo's works inspired Sunao Murashige and Takeshi Kinoshita [4] to theoretically investigate the conditions for an ideal wave focusing lens. They found that the sectional shape of the lens needs to give a large phase lag to the transmitted waves, namely greater than 2π. An array of submerged cylinders could satisfy this condition at high frequencies range. They also compared the performance of the bi-convex lens and Fresnel-type lens constructed from an array of submerged cylinders. The results showed that the bi-convex lens performed better in the context of waves' concentration. Later, elliptical lenses were investigated by using ray theory [5]. The lens comprises an elliptical plateau raised from the seabed instead of an array of cylinders. The theory was found to be a good approximation of the experimental results, and also elliptical lenses performed better than bi-convex lenses. However, all of the above structures are limited to directional waves. It is difficult to adapt theories to the anisotropic environment of the ocean.

The concepts of Fabry-Perot resonances used in optics were applied to water waves in 2018 by Chunyang Li, et al [6]. They experimentally and numerically demonstrated the effect of Fabry-Perot resonances in water waves with a scale device. In 2020, Zhigang Zhang et al. [7] used several truncated cylinders located at the perimeter of a circle to achieve an effect similar to the one observed by Chunyang Li. Because of the cylindrical symmetry, their device potentially performs for waves coming from different directions.

Gradient-index(GRIN) lenses serve as an alternative device that can manipulate the waves. GRIN lenses are the lenses that can produce optical effects by a material with a gradient of the refractive index. In recent decades, GRIN lenses have gained massive development in the field of optics [8]. However, the idea of utilizing GRIN lenses in the field of ocean energy to focus water waves has only just recently emerged. Wang et al. (2014)[9] first investigated the effects of focusing water surface waves via GRIN lenses experimentally and numerically. They observed that the results obtained from the experiment reasonably corresponded with the simulations. Nevertheless, the device's size and the water depth they tested are in the millimetre scale, where capillary effects need to be considered. It is unknown what the focusing effect of GRIN lenses performances would be up to the metre scale.

In this paper, we used the smoothed-particle hydrodynamics (SPH) approach to simulate the propagation of regular waves over a GRIN lens with hyperbolic secant profile, which is submerged in water with a depth of 10 cm.

II. Theory of wave focusing via a GRIN lens

Considering water as an incompressible and non-rotational fluid, the speed of a linear wave in shallow water is given by:

$$c = \sqrt{gH}, \tag{2.1}$$

where H is the water depth and g is gravity.

The refractive index, n, defined as the ratio of wave speeds in two media, can be easily manipulated by varying the water depth.

Let's consider that the wave is propagating in the x-direction. The refractive index in the region $x > 0$ is a function of y:

$$n = n(y), \quad x > 0. \tag{2.2}$$

If the water depth in region $x < 0$ is H_0, then the cross-sectional profile of the GRIN lens can be designed as:

$$z = H_0 - \frac{H_0}{n^2(y)}. \tag{2.3}$$

According to Fermat's principle, the optical length,S of a wave ray between two points (here denoted as P_1 and P_2 without loss of generality) is an extreme value:

$$\delta S = \int_{P_1}^{P_2} n(y)ds = 0, \tag{2.4}$$

where ds is a small distance of the wave ray.

This variation generally gives three Euler-Lagrange equations in x, y, and z components. But if the surface wave is propagating in the x-y plane and the refractive index is a function of y only, then the equation of the x component will reduce to:

$$\frac{d}{dx}\left(\frac{n(y)}{\sqrt{1+\left(\frac{dy}{dx}\right)^2}}\right) = 0 \tag{2.5}$$

Or,

$$\frac{n}{\sqrt{1+\left(\frac{dy}{dx}\right)^2}} = l_0, \tag{2.6}$$

where l_0 is a constant of integration from (2.5).

The general solution for (2.6) is:

$$x = \int_{y_0}^{y} \frac{l_0}{\sqrt{n^2(y') - l_0^2}}\, dy'. \tag{2.7}$$

In this study, we choose $n(y) = n_0 \operatorname{sech}(\alpha y)$. Then, the wave ray equation can be explicitly solved [10]:

$$y = \frac{1}{\alpha}\sinh^{-1}[\sinh(\alpha y_0)\cos(\alpha x) + m_0 \cosh(\alpha y_0)\sin(\alpha x)], \tag{2.8}$$

m_0 is the slope of the ray at $x = 0$ and α is a shape parameter that determines the steepness of the GRIN lens:

$$\alpha = \frac{2}{w}\cosh^{-1}(n_0), \tag{2.9}$$

w is the width of the GRIN lens, n_0 is the refractive index along the principal axis (i.e. y = 0). In this study, we fixed $n_0 = 1.5$ for all the cases.

Two special cases of (2.8), $m_0 = 0$ and $m_0 = \tan\theta$, are explored in the SPH simulation.

Case I: $m_0 = 0$

For a plane wave that enters the GRIN lens at $\theta = 0°$, all the incident rays will be trapped inside the lens and oscillate about the x-axis. The common point where all the rays converge is defined as the focal point, (x_f, y_f). Because of the symmetry about the x-axis, $y_f = 0$. From (2.8), we have:

$$\cos(\alpha x_f) = 0. \tag{2.10}$$

There are a series of focal positions along the principal axis and the focal positions are determined only by the steepness of the lens:

$$(x_f, y_f) = \left(\frac{N\pi}{2\alpha}, 0\right), \qquad N = 1,3,5 \ldots \tag{2.11}$$

In this study, the length of the GRIN lens, ℓ is designed in such a way that the GRIN lens is twice of the first focal length(N=1). Hence, it is expected that there will be a unique focal point in the lens. Fig. 1 shows the general dimensions of the GRIN lens used in this study.

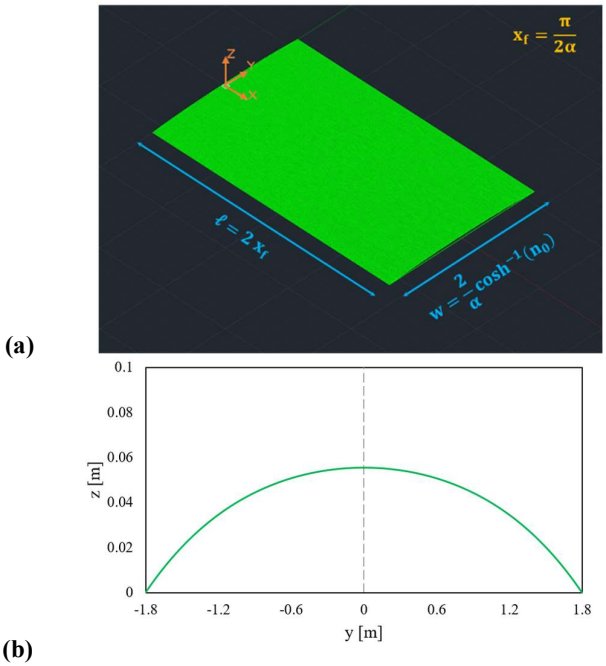

Figure 1. (a) The length of the GRIN lens is twice of the first focal length,$\ell = \pi/\alpha$. The width is determined by the steepness,α according to (2.9). (b) Cross-sectional profile of the GRIN lens with $\alpha = 0.535\ m^{-1}$.

Case II: $m_0 = \tan\theta$

For a plane wave that enters the GRIN lens with a constant slope of $m_0 = \tan\theta$ and $\theta \neq 0$, there is no common convergence point for all the rays. Every ray that enters from $+y_0$ will intercept with the ray that enters from $-y_0$ at the same x-position, x_f, but different y-positions. The furthest interception point is the interception of two rays from the boundaries, $y_0 = \pm w/2$. This causes the intensity of the wave at x_f to spread along the y-axis. Some of the rays that enter near the boundaries at an angle may even be lost, because once the rays leave the area of the lens, they will follow a straight path due to the constant refractive index outside the lens. As a result, the intensity of the wave is expected to be decreased when θ increases.

Although there is no common convergence point for the rays, we can define a general focal position by using the half distance of the furthest interception. From (2.8) we should have:

$$(x_f, y_f) = \left(\frac{N\pi}{2\alpha}, \quad \frac{1}{2\alpha}\left\{\sinh^{-1}\left[m_0 \cosh\left(\frac{\alpha w}{2}\right)\right]\right\}\right). \tag{2.12}$$

When $m_0 = 0$, (2.12) will recover (2.11).

III. Simulation setup

DualSPHysics is an open-source solver for the SPH approach developed by Gomez-Gesteira et al[11]. The solver incorporates C++ and CUDA codes which allow for parallel computing on the graphics processor unit (GPU). Many validations have been published[12-14] that indicate the versatility and reliability of the software. As such, we have adopted DualSPHysics as a tool in the study of the focusing of water surface waves caused by the GRIN lens.

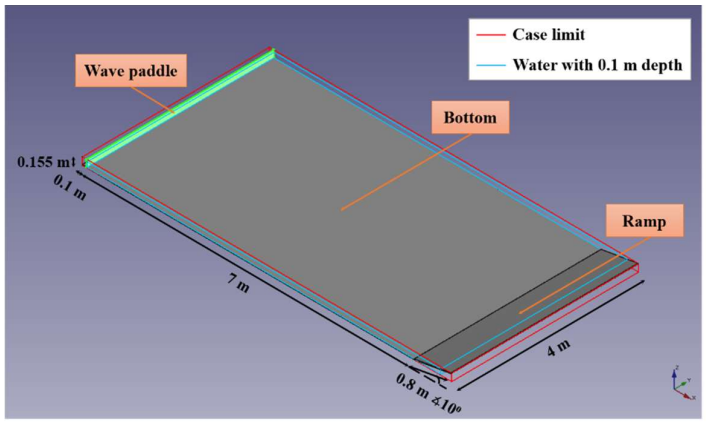

Figure 2. The dimensions of the water tank. The width of the tank is 4.0 m and the total length of the tank is 7.9 m, including a 0.8 m ramp with a 10° slope. A movable wall serves as a wave paddle at upstream of the tank.

The dimensions of the water tank we used are shown in Fig. 2. The width of the tank is 4.0 m, with periodic boundary conditions, and the total length of the tank is 7.9 m, including a 0.8 m ramp with a 10° slope. The ramp is designed to reduce the disturbance of reflected waves. A monochromatic wave with periodT, wave height A, and wavenumber k is generated by a wave paddle located upstream of the tank. The motion of the paddle is governed by:

$$e(t) = \frac{S_0}{2}\sin\left(\frac{2\pi}{T}t\right) + \frac{A^2}{32H_0}\left[\left(\frac{3\cosh(kH_0)}{\sinh^3(kH_0)}\right) - \frac{\sinh(kH_0)\cosh(kH_0) + kH_0}{\sinh^2(kH_0)}\right]\sin(\frac{4\pi}{T}t), \quad (3.1)$$

where S_0 is the stroke of the wave paddle[15]. The wave number,$k = \frac{2\pi}{L}$ is mathematically determined by the dispersion relation with given T and H_0

$$\frac{2\pi}{T} = \sqrt{gk\tanh(kH_0)}. \quad (3.2)$$

To evaluate the focusing effect of a GRIN lens, we first simulated the waves propagating across the tank without the GRIN lens for different wave periods and wave heights. Then, simulations with the same wave conditions were repeated with different steepness of the GRIN lens, placed at the centre of the tank. For the tests of different incident angles, the GRIN lens was rotated clockwise about the z-axis with an angle,θ. The controlled parameters used in the simulations are summarized in Table 1.

Table 1. The controlled parameters used in the simulations

Controlled parameters	Values
Wave period T[s]	0.7, 0.9, 1.1, 1.3, 1.5, 1.7, 1.9
Wave height A[m]	0.0075, 0.01, 0.015, 0.02, 0.025, 0.03
Steepness of GRIN lens $\alpha[m^{-1}]$	0.535, 0.611, 0.713, 0.855, 1.069
Incident angle θ[°]	0, 5, 10, 15, 20

In DualSPHysics, we need to choose an inter-particle distance, d_p to set up the initial position of particles. This value of d_p will determine the number of particles used in the simulation and crucially determine the time of computation. To compromise with a reasonable time of computation, we choose d_p = 0.0075 m, which gives roughly seven million particles in a simulation, and a total computation time for one simulation of around six hours with an RTX 3060 laptop GPU. The other fixed parameters used in the simulation are listed in Table. 2.[16]

Table 2. Fixed executive parameters defined in the simulation model

Execution parameters	Values
Smoothing length	0.013m
Artificial viscosity coefficient	0.01
Gravity	9.81m/s^2
Water density	1000kg/m^3
Coefficient for minimum time step	0.05
Time of simulation	15.0s
Time out data	0.1s
Step algorithm	Symplectic
Kernel	Wendland

IV. Post-data processing

After a plane wave enters the GRIN lens, the wavefront travels slower along the principal axis than along the edges due to the different water depths. As a consequence, the wave is deflected and converged to a region near the center of the lens (Fig. 3). To find the focal point from the simulation, we extracted the water surface elevation along the x-axis and y-axis at y=0 and x=x_f, respectively. Then, we calculate the average wave height, z_{rms} in the time interval, where the time is long enough for the wave to be fully developed and short enough to avoid significant disturbance from the reflected wave.

$$z_{rms} = \sqrt{8}\sigma_\eta, \tag{4.1}$$

where σ_η is the standard deviation of the water surface elevation time series data.

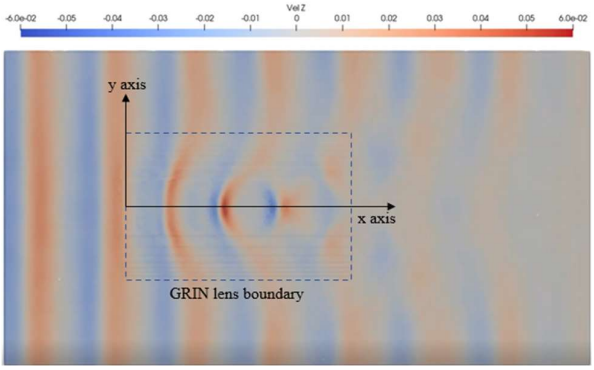

Figure 3. A typical wave pattern is given by SPH simulation. After the wavefront of a plane wave enters the GRIN lens, it travels slower along the principal axis but faster along the edges. As a consequence, the wave is deflected and converged.

As a plane wave, z_{rms} is uniformly distributed across the y-direction. But because of energy dissipation, it is generally decaying while the wave is propagating along the x-direction without the GRIN lens, as shown in Fig. 4. With the GRIN lens, the wave energy is gradually converging to the centre and a typical diffraction pattern with a central maximal is formed along the y-axis(Fig.4b). Hence, z_{rms} along the principal axis grows to a maximum value before it decays. The effect with the GRIN lens is the concentration of the uniform energy distribution into a smaller region.

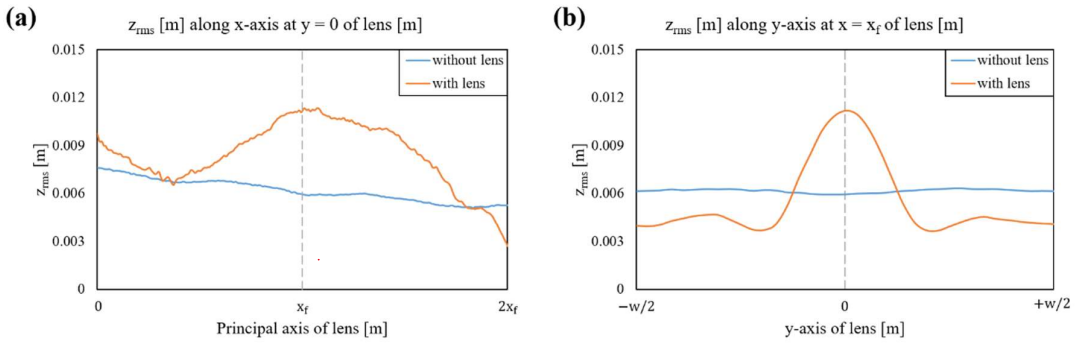

Figure 4. (a) The average wave height along the principal axis decays due to energy dissipation while propagating across the tank without the GRIN lens (blue line). With the GRIN lens, a maximal occurs near the focal position (orange line). (b) The average wave height along the y axis at $x = x_f$ is nearly constant without the GRIN lens (blue line). After the GRIN lens is added, a diffraction pattern is formed (orange line).

Since wave intensity is proportional to z_{rms}^2 , we can obtain the relative wave intensity, I_R by comparing z_{rms}^2 with and without the GRIN lens under the same wave conditions.

$$I_R = \frac{z_{rms}^2 \; with \; lens}{z_{rms}^2 \; without \; lens}. \tag{4.2}$$

We denote β as the maximum value of I_R inside the region of the GRIN lens. The position of β defines the focal position predicted by SPH simulation. If $\beta > 1$, then the wave is amplified. Therefore, we call β the amplification factor of the wave.

V. Results And Discussion

According to the prediction given by (2.11), x_f is inversely proportional to α and independent from the wave parameters. Fig. 5(a) and (b) show good agreement between the simulation results and the theoretical predictions within 5% of error. However, when wave steepness was greater than 0.012, the focal position was deviated from the prediction as Fig. 5(c) shown. This is because wave speed is not simply determined by the water depth when the wave height is large. The speed of the wavefront along the principal axis could be increased as the wave height grows. In this case, when the wave height exceeded about 10% of the still water depth, the focusing of the wave was delayed.

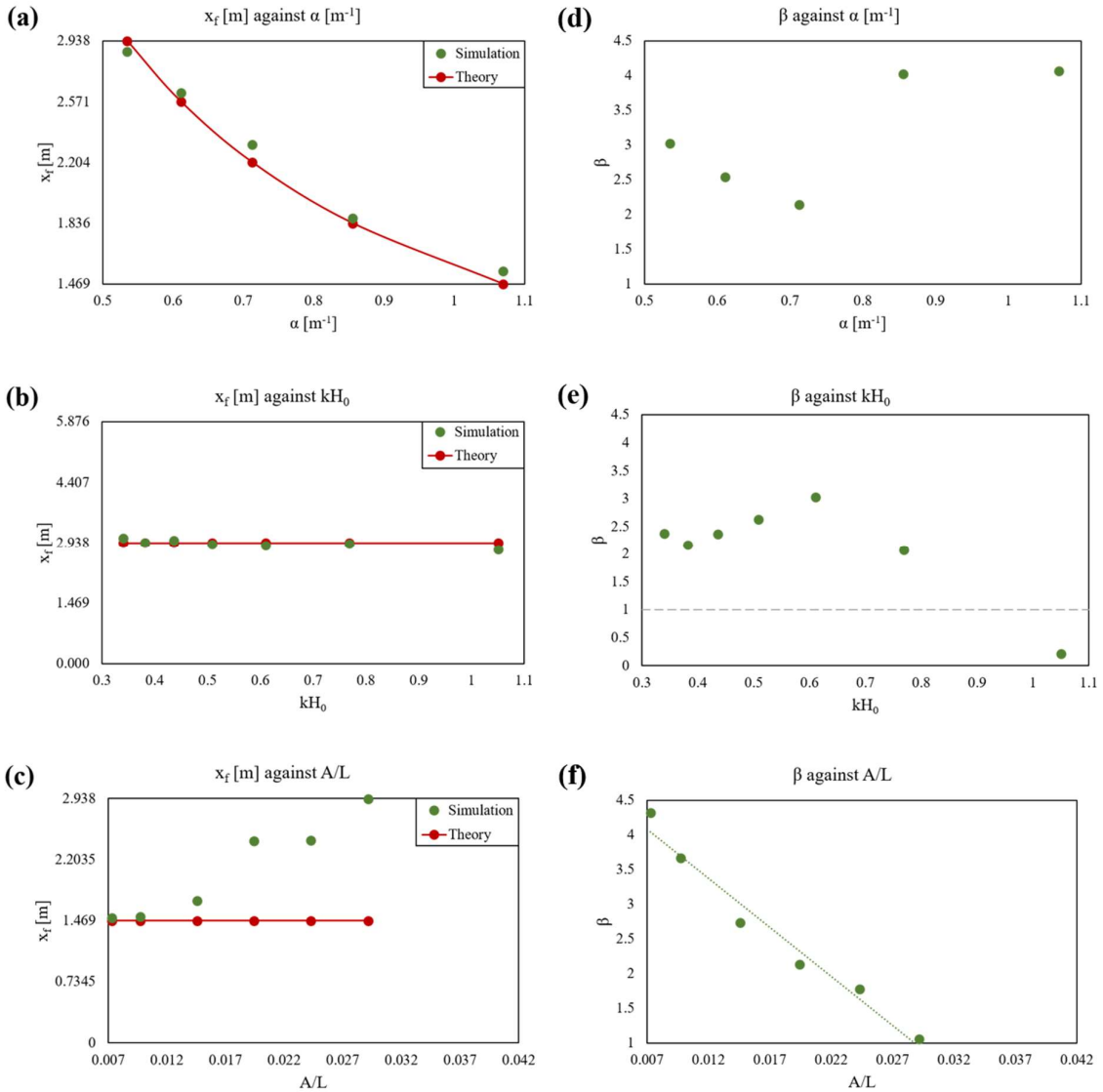

Figure 5. (a)-(c) Shows the comparison of the focal positions predicted by SPH simulation (dark green dots) and rays theory (red dots). (a) Focal position as a function of GRIN lens steepnessαat kH_0 = 0.6107, A/L = 0.0073 (b) Focal position as a function of relative water depth kH_0 at A/L = 0.0073,α = 0.535 m^{-1}, and (c) Focal

position as a function of wave steepnessA/Lat $kH_0 = 0.6107$, $\alpha = 1.069\ m^{-1}$. (d)-(f) Shows the amplification factors corresponding to (a)-(c). The amplification factor drops to unity when the relative water depth in (e) and the wave steepness in (f) get larger than a threshold.

When GRIN lens steepness varied from 0.5 m^{-1} to 1.1 m^{-1}, the amplification factor fluctuated around 2.0 to 4.0. No significant trend could be concluded from the data(Fig.5(d)). However, the amplification factor was indeed significantly affected by the relative water depth and wave steepness. When the wave steepness was fixed at 0.0073, the amplification effect vanished when the relative water depth exceeded 0.9 as shown in Fig.5(e). This criterion is equivalent to a deviation of about 10% from the shallow water limit condition. When the relative water depth was fixed at 0.61, the amplification factor decreased linearly and across $\beta = 1$, around A/L=0.028(Fig.5(f)). This implies that the amplification effect will disappear when the nonlinearity of the wave increases. So far, no theory has predicted how the relative water depth and wave steepness affect the amplification factor. The simulation results in this paper favour that the amplification only happens when both the shallow water and linear wave conditions are fulfilled.

When the incident wave had an angle, θ with the principal axis of the GRIN lens, the focal position shifted along y-axis but the x-position remained unchanged. Fig. 6 shown the theoretical ray trajectories and simulated wavefronts at different wave incident angles. The trajectories were represented by a series of curves given by (2.8), and the background colour map shown the distribution of water surface velocities in z component extracted from the simulations. The positions where the rays converged were well agreed with the highest water surface speed region. To quantify the shifts of focal position due to different incident angles, the relative wave intensity, I_R along y-axis at $x=x_f$ were plotted in Fig. 7(a). The maximum of $I_R$occurred at y = 0 as expected when $\theta=0$. As θ increases, the shifts of the focal position were well predicted by (2.12)(Fig.7(b)).

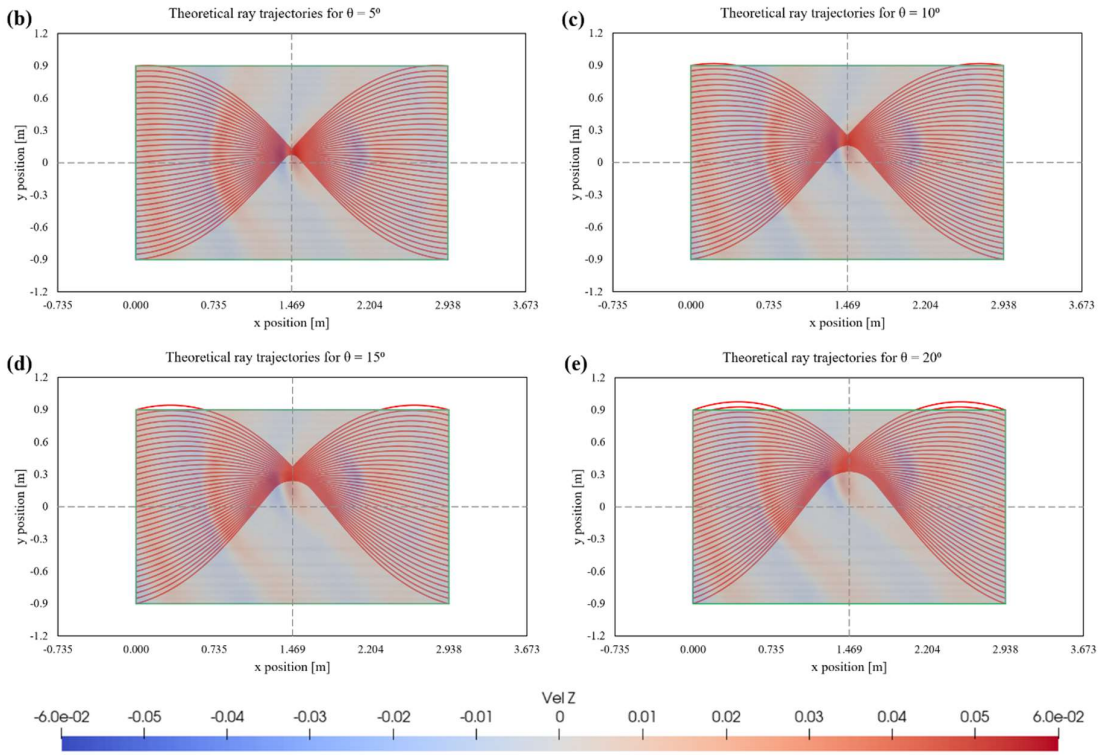

Figure 6. Comparison of the wavefronts from SPH simulation and the wave rays predicted by ray theory at different incident angles, θ. A/L=0.0097, kH_0=0.6107, $\alpha = 1.069\ m^{-1}$. The red lines are the path of the rays given by (2.8). The colour map behind the rays is the z component of the water surface velocity given by SPH simulation.

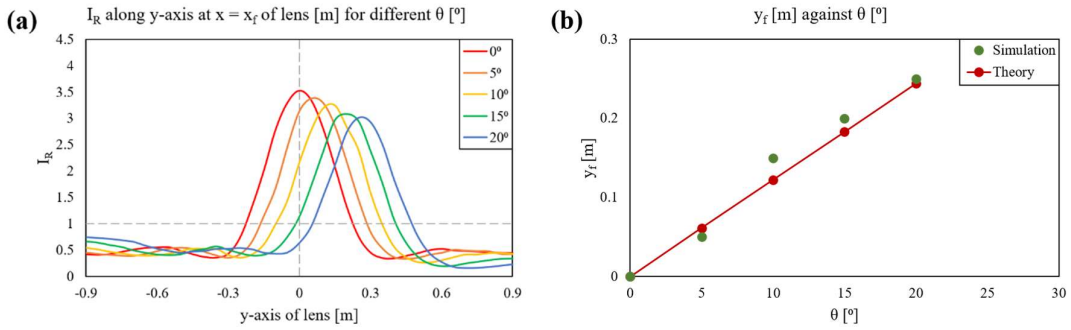

Figure 7. (a) The relative wave intensity along the y axis at $x=x_f$ shows a typical diffraction pattern. The central maximal of the intensity shifts to right when the incident wave angle increases. (b) The position of the central maximal as a function of incident wave angle (dark green dots). The red line is the general focal position predicted by (2.12).

VI. Conclusion

This study showed that gradient-index (GRIN) lens can be used to manipulate the propagation of water surface wave and concentrate the wave energy in a pre-designed region. The focusing of the wave is well predicted by GRIN optics The amplification factor retains above 2 even the incident angle is 20°. However, it is discovered that the amplification of the waves only happens when both the linear wave (i.e. A << L) and shallow-water conditions (i.e. kH << 1) are satisfied. To break this limitation, a GRIN lens with non-uniform steepness is currently under investigating

References

[1]. G. Wolters, G. Muller, Tom Bruce, Charlotte Obhral, Large-scale experiments on wave downfall pressures. Maritime Engineering 158, issue MA4 (2005) pp137-145.https://doi.org/10.1680/maen.2005.158.4.137.
[2]. J.J. Stamnes, O. Lovhaugen,B. Spjelkavik, Chiang C. Mei, E. Lo, and D.K.P. Yue, Nonlinear focusing of surface waves by a lens-Theory and experiment. J. Fluid Mech. (1983) Vol. 135, 71-94. https://doi.org/10/1017/S0022112083002967.
[3]. Kudo K., Tsuzuki T., Imai K., and Akiyama Y., Study on wave focusing by a horizontally submerged plate. J. Soc. Nav. Arch. Japan, 160 (1986) 217-225. https://doi.org/10.2534/jjasnaoe1968.1986.160_217
[4]. S. Murashige and T. Kinoshita, An ideal ocean wave focusing lens and its shape. Applied Ocean Research 14 (1992) 275-290. https://doi.org/10.1016/0141-1187(92)90032-F.
[5]. L.S. Griffiths, R. Porter, Focusing of surface waves by variable bathymetry. Applied Ocean Research 34 (2012) 150-163.https://doi.org/10.1016/j.apor.2011.08.004.
[6]. Chunyang Li, Lin Xu, Loli Zhu, Siyuan Zou, Qing Huo Liu, Zhenyu Wang, and Huanyang Chen, Concentrators for Water Waves. Phys. Rev. Lett. 121 (2018) 104501.https://doi.org/10.1103/PhysRevLett.121.104501.
[7]. Zhigang Zhang, Shuang Liu, Zhengxiao Luan, Zhengke Wang, and Guanghua He. Invisibility concentrator for water waves.Phys. Fluid, 32 (2020) 081701. https://doi.org/10.1063/5.0019129.
[8]. Hyun, J., Choi, W., and Kim, M., Gradient-index phononic crystals for highly dense flexural energy harvesting. Applied Physics Letters, 115(17) (2019) 173901. https://doi.org/10.1063/1.5111566.
[9]. Wang, Z., Zhang, P., Nie, X., & Zhang, Y. (2014). Focusing of liquid surface waves by gradient index lens. EPL 108(2014) 24003. https://doi.org/10.1209/0295-5075/108/24003
[10]. C. Gomez-Reino, M.V. Perez, and C. Bao, Gradient-Index Optics.Springer(2002)https://doi.org/10.1007/978-3-662-04741-5.
[11]. Crespo AJC, Domínguez JM, Rogers BD, Gómez-Gesteira M, Longshaw S, Canelas R, Vacondio R, Barreiro A, García-Feal O, DualSPHysics: open-source parallel CFD solver on Smoothed Particle Hydrodynamics (SPH). Computer Physics Communications, 187: (2015) 204-216. https://doi.org/10.1016/j.cpc.2014.10.004
[12]. Zhang F, Crespo AJC, Altomare C, Domínguez JM, Marzeddu A, Shang S, Gómez-Gesteira M., DualSPHysics: a numerical tool to simulate real breakwaters. Journal of Hydrodynamics, 30(1) (2018) 99-105. https://doi.org/10.1007/s42241-018-0010-0.
[13]. González-Cao J, Altomare C, Crespo AJC, Domínguez JM, Gómez-Gesteira M, Kisacik D., On the accuracy of DualSPHysics to assess violent collisions with coastal structures. Computers & Fluids, 179 (2019) 604-612. https://doi.org/10.1016/j.compfluid.2018.11.021.
[14]. Jun Zeng, Jia Shen, and Haijiang Liu, A parametric study of Dam Break flow feature over a dry bed using SPH Modeling. Proceedings of the 10th International Conference on Asian and Pacific Coasts (2019) 25-28. https://doi.org/10.1007/978-981-15-0291-0_12.
[15]. O.S. Madsen, Waves Generated by a Piston-type Wavemaker. Costal Engineering Proceedings (1970) https://doi.org/10.9753/icce.v12.36.
[16]. User Guide for DualSPHysics code, Home · DualSPHysics/DualSPHysics Wiki · GitHub
[17]. Heller, V. (2012). Development of wave devices from initial conception to commercialdemonstration. In Comprehensive Renewable Energy. https://doi.org/10.1016/B978-0-08-087872-0.00804-0